Thin Flexible Pressure Sensor Array Based on Carbon Black/Silicone Rubber Nanocomposite

Luheng Wang, Tianhuai Ding, and Peng Wang

***Abstract*—In this paper, the key technologies for the development of the thin flexible pressure sensor array based on carbon black/silicone rubber nanocomposite are reported. The piezoresistive mechanism of the nanocomposite is explained by analyzing the changes in effective conductive paths. The technical data of the sensor system are given. With the measurement range of 0–1 MPa, the maximum measurement deviation is less than 30 kPa.**

***Index Terms*—Carbon black, piezoresistance, polymer composite, sensors.**

I. Introduction

THE pressure measurement has great significance in the fields of aerospace engineering, automobile making, robot tactility, etc. [1]–[6]. In some engineering application, due to the complication of surface configuration and the smallness of interlayer spacing, the pressure sensor is required to be flexible and thin. For example, in our previous engineering project, we developed a small interlaminar monitoring system [7], [8]. The maximum interlayer gap spacing is 2 mm. The thickness of the sensor is required to be less than 0.13 mm due to the existence of a thin substrate. Besides, the engineering requirements for the pressure monitoring include the following: the load pressure range is 0–1 MPa, the maximum measurement deviation is 30 kPa, the temperature range is 23 °C–30 °C, and the moisture range is 50%–70% relative humidity (RH).

The electrical resistance of conductive polymer composite changes with external pressure regularly [9]–[21]. Therefore, this kind of material can be used as the sensing element of pressure sensor [22]–[29]. However, most research results have been not applied to engineering practice, and some pressure sensors based on this kind of material still need to be improved or adjusted according to the specific requirements of engineering applications. For example, the researchers in the Industrial Products Research Institute of Japan [6] successfully developed a tactile sensor based on conductive rubber. However, the sensor is mainly used to measure pressure distribution, and the thickness of the sensor is 0.5 mm, which is too thick to satisfy the engineering requirement (< 0.13 mm). So *et al.* [22] successfully developed a touch sensor design based on the conductive rubber, which is used to determine the shape of an object in contact with the sensor. However, due to quantization errors and sensor noise, the extent of inaccuracy is being examined. Shimojo *et al.* [23] developed a sheet-type tactile sensor using pressure conductive rubber with electrical-wires stitches method. However, the measurement range is 0–0.2 MPa, which does not satisfy the requirement of engineering application (0–1 MPa).

Under the circumstances, a cheap flexible pressure sensor with high accuracy and suitable thickness is needed urgently. Tekscan sensors can have a thickness of 100 μm, are flexible, and a high spatial resolution with thousands of sensing points. Further, they can be used to measure pressures from 0.05, or lower, up to 150 MPa, or higher. These commercial sensors provide accuracies of around 1% if calibrated. In this paper, an alternative method to make such a sensor is provided. A low-cost method for the development of thin (0.125 mm) flexible pressure sensor array is reported. Carbon black/silicone rubber nanocomposite, with piezoresistivity and flexibility, is used as the sensing element of the sensor. The piezoresistive mechanism of the composite is explained qualitatively. The fabrication of pressure-sensitive nanocomposite, the design of signal processing system, and the development of calibration/fitting method are reported. The key technical data of the sensor are also given.

II. Development of the Pressure Sensor

A. Preparation of the Sensing Element

Fig. 1 shows the preparation process of the sensing element. Room temperature vulcanized liquid silicone rubber (107, Beijing Chemical Plant, China) and conductive carbon black powder (SL36, Carbon Black R&D Institute, China) are used as insulating matrix and conductive phase, respectively. The properties of the rubber matrix and the carbon black found in the manufacturer literatures are presented in Table I. Through many experiments on the piezoresistivity of the nanocomposites with different conductive phase content, we draw the conclusions as follows. If the mass ratio of carbon black to silicone rubber is less than 0.06:1, the resistance value is too large to design circuits easily. If the mass ratio is higher than 0.10:1, the piezoresistivity is nonmonotonous. The best range of mass ratio is from 0.07:1 to 0.09:1. The mass ratio used in this paper is 0.08:1. Hexane is used as solvent to mix the fillers with the rubber. The volume ratio of hexane to silicone rubber is 40:1. Mechanical stirring along with ultrasonic vibration is also used for better particle dispersion. The ultrasonic power and the ultrasonic frequency of the ultrasonic cleaner (RSQ-30AS) are 300 W and 40 kHz, respectively. The mechanical stirrer

Manuscript received November 06, 2008; revised December 16, 2008 and January 20, 2009; accepted March 02, 2009. Current version published August 21, 2009. The associate editor coordinating the review of this paper and approving it for publication was Prof. Gerald Gerlach.

L. Wang is with the College of Information Science and Engineering, Northeastern University, Shenyang 110004, China (e-mail: wlh03@mails.tsinghua.edu.cn).

T. Ding and P. Wang are with the State Key Laboratory of Precision Measurement Technology and Instruments, Department of Precision Instruments and Mechanology, Tsinghua University, Beijing 100084, China (e-mail: wlh03@mails.tsinghua.edu.cn).

Digital Object Identifier 10.1109/JSEN.2009.2026467

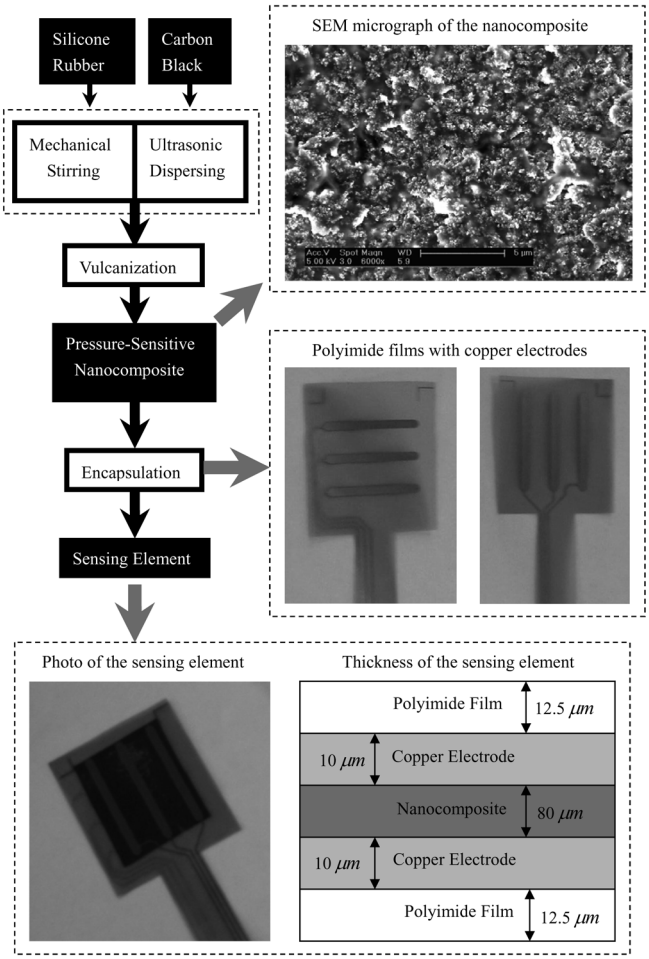

Fig. 1. Preparation process for the sensing element.

TABLE I
PROPERTIES OF CARBON BLACK AND SILICONE RUBBER

	Specific surface area (m^2/g)	Resistivity ($\Omega \cdot cm$)	Young's Modulus (MPa)	Dielectric constant
Carbon Black	780	0.2	1.5×10^5	
Silicone Rubber		1.0×10^{14}	6	3.0

(IKA RW20n) is set to 180 r/min. The solvent is evaporated naturally during the agitation process. After 5 h of vigorous mixing, the mixture becomes viscous status. The viscous mixture is made into a thin film by spin coating. The viscous film is vulcanized at 30 °C for 40 h. The SEM micrograph of the fractured surface for the nanocomposite is also shown in Fig. 1, showing a good dispersion of carbon black particles in the silicone rubber matrix.

The vulcanized film is encapsulated between two polyimide films with copper electrodes. As shown in Fig. 1, there are three pieces of lateral electrodes on one polyimide film, and there are three pieces of longitudinal electrodes on the other polyimide film. The nine intersections between the lateral and longitudinal electrodes constitute nine sensing elements of the pressure sensor. The thickness of the polyimide films, copper electrodes, and pressure-sensitive nanocomposite are also shown in Fig. 1. The total thickness of the encapsulated sensing element is $125\,\mu$m.

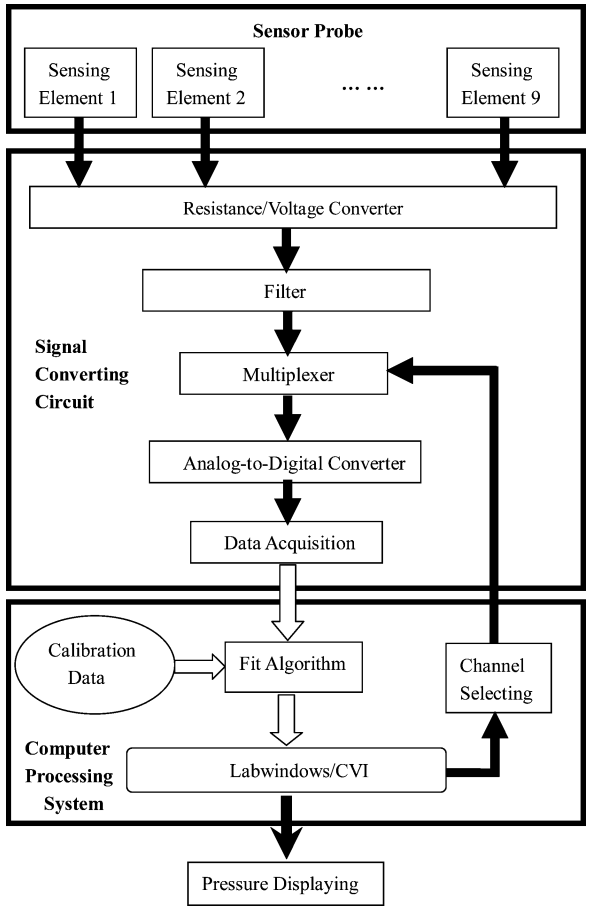

Fig. 2. Sketch of the signal processing system.

B. Signal Processing System

The sketch for signal processing system is shown in Fig. 2. The resistance signals of the nine sensing elements are converted to voltage signals. Then, the voltage signals are inputted into a multiplexer after filtering. The channel of the multiplexer is selected by the control signal of a microcomputer. After this, the selected voltage signal is converted to digital signal through A/D converter. The digital signal is inputted into the computer through the data acquisition system. The analyzing, processing, and displaying of the nine signals are realized by using Labwindows/CVI.

III. CALIBRATION BASED ON PIEZORESISTIVITY

A. Piezoresistive Mechanism of the Nanocomposite

Fig. 3(a) shows the shell structure model of the carbon black/silicone rubber nanocomposite [30]. Phase A is a rubber molecule chain with active micro-Brownian motion, which is not adsorbed by carbon black; phase B is a cross-linked rubber molecule chain, the motion of which has been restricted; phase C is a macrorubber molecule chain with low level of activity, which is adsorbed on the surface of carbon black through physisorption and chemisorption; phase D is a carbon black. Elastic phases A and B are bonded to phase C, which acts as a framework,

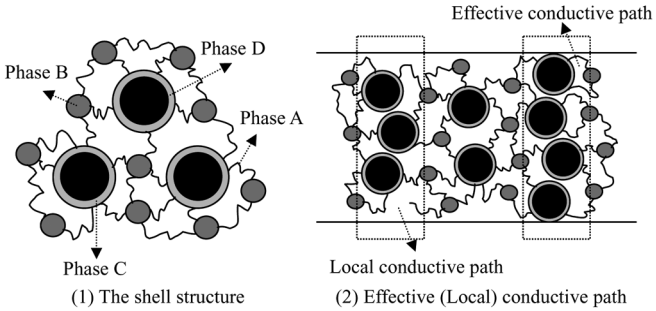

Fig. 3. Schematic diagram for the inner structure of nanocomposite.

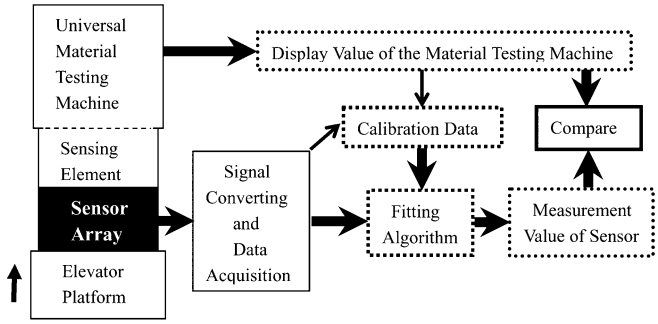

Fig. 4. Sketch map of the testing system.

forming a 3-D network composed of carbon black and rubber macromolecule.

When the gap between carbon black particles is small enough to make them touch or come close to each other, contact effect and tunneling effect occur, leading to the formation of local conductive path. If the local conductive path penetrates the insulating matrix, an effective conductive path is formed, thus contributing to the conductivity of composite. The schematic view of the local conductive path and the effective conductive path are shown in Fig. 3(b).

Carbon black is incompressible compared with silicone rubber [30]. Therefore, the compression can induce translation and rotation of carbon black, leading to the changes in effective conductive path as follows.

1) Change in One Effective Conductive Path: The uniaxial pressure makes the gaps between two adjacent conductive particles smaller, decreasing the electrical resistance of one effective conductive path.

The electrical resistance of one single effective conductive path can be described by [31]

$$R = \frac{2h^2 sL}{3a^2 e^2 \sqrt{2m\varphi}} \exp\left(4\pi \sqrt{2m\varphi}\frac{s}{h}\right) \tag{1}$$

where R is the resistance of a single effective conductive path, L the number of particles forming one conductive path, m the electron mass, e the electron charge, h the Plank's constant, s the thickness of insulating film, φ the height of potential barrier between adjacent particles, and a^2 the effective cross-sectional area, where the tunneling effect occurs.

As shown in (1), the decrease of s, caused by uniaxial pressure, leads to the decrease of R. That is to say, the gaps between carbon black particles get smaller and smaller during compression, leading to the increase of the tunneling current, which decreases the resistance of one single effective conductive path.

2) Formation of Effective Conductive Paths: The compression makes the gaps between carbon black particles smaller, leading to the formation of effective conductive paths. This effect contributes to the increase of the number of effective conductive paths.

3) Destruction of Effective Conductive Paths: The transverse slippage of carbon black, caused by compression, leads to the destruction of effective conductive paths. This effect contributes to the decrease of the number of effective conductive paths.

The three kinds of changes aforementioned concur during compression. The changes (1) and (2) contribute to the decreasing tendency of composite resistance. The change (3) contributes to the increasing tendency of composite resistance.

The secondary structure composed of carbon black by Van der Waals forces is unstable. Therefore, the compression can change the unstable structure, leading to the unrecoverable damage of conductive network. However, with the increase of compression cycles, the structure of the carbon black network becomes steady, leading to the gradual stable relation between the composite resistance and the applied pressure [12]. Therefore, the nanocomposite can be used as the sensing element of the pressure sensor.

B. Experimental Sets

The experimental sets shown in Fig. 4 can be used for sensor calibration and comprehensive performance test. The sensor array is placed between the elevator platform and the sensing element of universal material testing machine. The sensor is applied to a given pressure through the uniaxial move of the elevator platform. The load pressure ranges from 0 to 1 MPa. The pressure value is recorded by the universal material testing machine. The electrical resistance is measured through the digital data acquiring system. The values of the pressure and the electrical resistances of the nine sensing elements are used as calibration data.

C. Calibration and Fitting

The piezoresistivities of nine sensing elements are all monotonically increasing. Take one of them as an example, the relation between the electrical resistance and the applied pressure is shown in Fig. 5. A total of ten data points are used as the calibration data.

The pressure P can be given by

$$P = s_{i+1} - \left(\frac{r_{i+1} - R}{r_{i+1} - r_i}\right) \times (s_{i+1} - s_i), \quad i = 0, 1, 2 \ldots, 9 \tag{2}$$

where R is the electrical resistance under pressure P, and r_i and s_i are the resistance value and the pressure value of the ith group of the calibration data, respectively.

IV. Performances of the Pressure Sensor

A. Conditions for Performance Test

The nine sensing elements of the sensor are tested after 12 precompression cycles. The load range is 0–1 MPa. The tem-

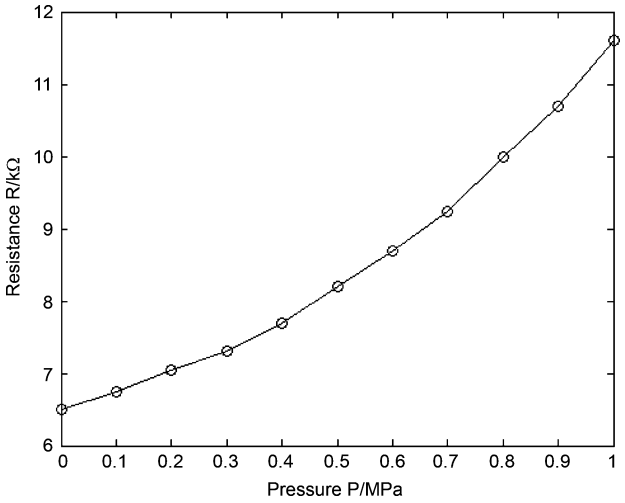

Fig. 5. Piezoresistivity of the nanocompoiste.

perature and the moisture of the performances test (nonlinear error, hysteresis error, repeatability error, resolution, and time drift) are 26 °C and 60% RH, respectively.

B. Nonlinear Error

As shown in Fig. 5, there are ten fitting straight lines for each sensing element. Therefore, the nonlinear error γ_N can be calculated as

$$\gamma_N = \frac{\pm \mathrm{Max}\{|\Delta N_{1\,\max}|, \ldots, |\Delta N_{10\,\max}|\}}{Y_{\mathrm{FS}}} \times 100\% \quad (3)$$

where $\Delta N_{j\,\max}$ is the maximum deviation of a real transfer function from the jth fitting straight line, $j = 1, 2, \ldots 10$, and Y_{FS} is the the measuring range.

The nonlinear errors for the nine channels of the sensor are shown in Fig. 6(a). We can see that the nonlinear error of the sensor is less than 0.12%

C. Hysteresis Error

The nine sensing elements are loaded from 0 to 1 MPa, and then are unloaded from 1 to 0 MPa. The maximum deviation between the load output and the unload output is marked as $\Delta H_{\max}$. The hysteresis error γ_H is calculated as

$$\gamma_H = \pm \frac{\Delta H_{\max}}{2Y_{FS}} \times 100\%. \quad (4)$$

The hysteresis errors for the nine channels of the sensor are shown in Fig. 6(b). We can see that the hysteresis error of the sensor is less than 1.3%.

D. Repeatability Error

The nine sensing elements of the sensor are loaded and unloaded for six cycles. The data of the electrical resistance and the pressure are recorded. The maximum deviation among six loading curves and that among six unloading curves are marked

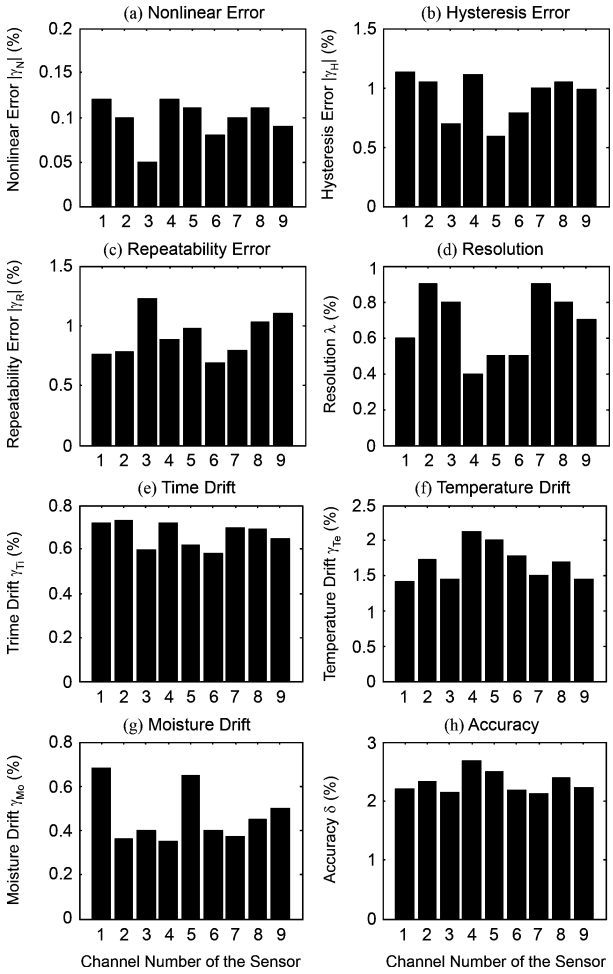

Fig. 6. Performances of the sensor.

as $\Delta R_{L\,\max}$ and $\Delta R_{U\,\max}$, respectively. The repeatability error γ_R can be calculated as

$$\gamma_R = \pm \frac{\mathrm{Max}\{|\Delta R_{L\,\max}|, |\Delta R_{U\,\max}|\}}{Y_{FS}} \times 100\%. \quad (5)$$

The repeatability errors for the nine channels of the sensor are shown in Fig. 6(c). We can see that the repeatability error of the sensor is less than 1.4%.

E. Resolution

The smallest magnitude of the input variation that can be measured by the sensor system is marked as ΔP. The resolution λ can be calculated as follows:

$$\lambda = \frac{\Delta P}{Y_{\mathrm{FS}}} \times 100\%. \quad (6)$$

The resolutions for the nine channels of the sensor are shown in Fig. 6(d). We can see that the resolution of the sensor is less than 0.9%.

F. Time Drift

The sensor under a certain pressure (0–1 MPa) is tested for 120 h. The output value of the sensor is recorded. The maximum deviation of the output value is marked as $\Delta Ti_{\max}$. The time drift γ_{Ti} can be calculated as follows:

$$\gamma_{Ti} = \frac{\Delta Ti_{\max}}{Y_{FS}} \times 100\%. \tag{7}$$

The time drifts for the nine channels of the sensor are shown in Fig. 6(e). We can see that the time drift of the sensor is less than 0.8%.

G. Temperature Drift

The sensor is taken into the environment box (ESPEC PR-3G). The test conditions are 1 standard atmosphere pressure and 60% RH. The temperature is increased from 0 °C to 40 °C. The maximum deviation of the output of the sensor system is marked as $\Delta Te_{\max}$. The temperature drift γ_{Te} can be calculated as

$$\gamma_{Te} = \frac{\Delta Te_{\max}}{Y_{FS}} \times 100\%. \tag{8}$$

The temperature drifts for the nine channels of the sensor are shown in Fig. 6(f). We can see that the temperature drift of the sensor is less than 2.4%.

H. Moisture Drift

The sensor under the zero pressure is taken into the environment box (ESPEC PR-3G). The test conditions are 1 standard atmosphere pressure and 26 °C. The moisture is increased from 30% to 90% RH. The maximum deviation of the output of the sensor system is marked as $\Delta M_{\max}$. The moisture drift γ_{Mo} can be calculated as

$$\gamma_{Mo} = \frac{\Delta M_{\max}}{Y_{FS}} \times 100\%. \tag{9}$$

The moisture drifts for the nine channels of the sensor are shown in Fig. 6(g). We can see that the moisture drift of the sensor is less than 0.7%.

I. Accuracy

The accuracy δ can be calculated as

$$\delta = \sqrt{\gamma_N^2 + \gamma_H^2 + \gamma_R^2 + \gamma_{Ti}^2 + \gamma_{Te}^2 + \gamma_{Mo}^2}. \tag{10}$$

The accuracies for the nine channels of the sensor are shown in Fig. 6(h). We can see that the accuracy of the sensor is 3%.

J. Comprehensive Test Results

The comprehensive test setup is also shown in Fig. 4. The pressure value is recorded by the universal material testing machine and the sensor array, respectively. The pressure values measured by the sensor array are compared with that displayed by the material testing machine to get the comprehensive testing results of the sensor. The sensor array is tested with the measurement range of 0–1 MPa. The temperature ranges from 23 °C to 30 °C, and the moisture ranges from 50% to 70% RH. The maximum measurement deviation of the sensor is 25 kPa.

V. Conclusion

The thin flexible pressure sensor array based on the carbon black/silicone rubber nanocomposite is fabricated and tested. The total thickness of the sensor is 125 μm. The nonlinear error is 0.12%, the hysteresis error is 1.3%, the repeatability error is 1.4%, the resolution is 0.9%, the time drift is 0.8%, the temperature drift is 2.4%, and the moisture drift is 0.7%. With the measurement range of 0–1 MPa, the maximum measurement deviation is 25 kPa.

The temperature range and the moisture range of the test fall within the scope of the engineering conditions (temperature range: 23 °C–30 °C; moisture range: 50%–70% RH). The measurement range, the accuracy, and the sensor thickness, all satisfy the requirements of the engineering application (load pressure range: 0–1 MPa; maximum measurement deviation: 30 kPa; sensor thickness: 0.130 mm). The low fabrication cost also meets the demands of the clients.

The area, the thickness, and the number of sensing elements of the pressure sensor can be adjusted according to different requirements in other engineering applications, such as the artificial skin, the finger-tip haptics of the robotic, etc.

References

[1] V. J. Lumelsky, M. S. Shur, and S. Wagner, "Sensitive skin," *IEEE Sensors J.*, vol. 1, no. 1, pp. 41–51, Feb. 2001.

[2] L. H. Wang, T. H. Ding, and P. Wang, "Effects of conductive phase content on critical pressure of carbon black filled silicone rubber composite," *Sens. Actuators A, Phys.*, vol. 135, no. 2, pp. 587–592, 2007.

[3] M. Shimojo, A. Namiki, M. Ishikawa, R. Makino, and K. Mabuchi, "A tactile sensor sheet using pressure conductive rubber with electrical-wires stitched method," *IEEE Sensors J.*, vol. 4, no. 5, pp. 589–596, Oct. 2004.

[4] T. H. Ding, L. H. Wang, and P. Wang, "Changes in electrical resistance of carbon black filled silicone rubber composite during compression," *J. Polym. Sci. B, Polym. Phys.*, vol. 45, no. 19, pp. 2700–2706, 2007.

[5] T. V. Papakostas, J. Lima, and M. Lowe, "A large area force sensor for smart skin applications," in *Proc. IEEE Sensors*, Orlando, FL, 2002, pp. 1620–1624.

[6] M. Shimojo, M. Ishikawa, and K. Kankaya, "A flexible high resolution tactile imager with video signal output," in *Proc. IEEE Int. Conf. Robot. Autom.*, Sacramento, CA, 1991, pp. 384–391.

[7] X. L. Chen, T. H. Ding, and Y. P. Huang, "Novel flexible eddy current array sensor system for proximity sensing," *Chin. J. Mech. Eng.*, vol. 42, no. 8, pp. 150–153, 2006.

[8] T. H. Ding, X. L. Chen, and Y. P. Huang, "Ultra-thin flexible eddy current sensor array for gap measurements," *Tsinghua Sci. Technol.*, vol. 9, no. 6, pp. 667–671, 2004.

[9] M. Hussain, Y. H. Choa, and K. Niihara, "Fabrication process and electrical behavior of novel pressure-sensitive composites," *Composties A*, vol. 32, no. 4, pp. 1689–1696, 2001.

[10] Q. Zheng, J. F. Zhou, and Z. H. Song, "Time-dependent uniaxial piezoresistive behavior of high-density polyethylene/shot carbon fiber conductive composites," *J. Mater. Res.*, vol. 19, no. 9, pp. 2625–2634, 2004.

[11] K. P. Sau, D. Khastgir, and T. K. Chaki, "Electrical conductivity of carbon black and carbon fibre filled silicone rubber composites," *Angew. Makromol. Chem.*, vol. 258, pp. 11–17, 1998.

[12] L. H. Wang, T. H. Ding, and P. Wang, "Effects of compression cycles and pre-compression pressure on repeatability of piezoresistivity for carbon-black-filled silicone rubber composite," *J. Polym. Sci. B, Polym. Phys.*, vol. 46, no. 11, pp. 1050–1061, 2008.

[13] X. J. Wang and D. D. L. Chung, "Short carbon fiber reinforced epoxy coating as a piezoresistive strain sensor for cement mortar," *Sens Actuators A, Phys.*, vol. 71, no. 3, pp. 208–212, 1998.

[14] M. H. El-Eraki, A. M. Y. El-Lawindy, H. H. Hassan, and W. E. Mahmoud, "The physical properties of pressure sensitive rubber composites," *Polym. Degrad. Stab.*, vol. 91, no. 7, pp. 1417–1423, 2006.

[15] J. J. C. Busfield, A. G. Thomas, and K. Yamaguchi, "Electrical and mechanical behavior of filled rubber. III. Dynamic loading and the rate of recovery," *J. Polym. Sci. B, Polym. Phys.*, vol. 43, pp. 1649–1661, 2005.
[16] K. Yamaguchi, J. J. C. Busfield, and A. G. Thomas, "Electrical and mechanical behavior of filled elastomers. I. The effect of strain," *J. Polym. Sci. B, Polym. Phys.*, vol. 41, pp. 2079–2089, 2003.
[17] J. J. C. Busfield, A. G. Thomas, and K. J. Yamaguchi, "Electrical and mechanical behavior of filled elastomers 2: The effect of swelling and temperature," *J. Polym. Sci. B: Polym. Phys.*, vol. 42, pp. 2161–2167, 2004.
[18] X. W. Zhang, Y. Pan, Q. Zheng, and X. S. Yi, "Time dependence of piezoresistance for the conductor-filled polymer composites," *J. Polym. Sci. B, Polym. Phys.*, vol. 38, pp. 2739–2749, 2000.
[19] F. G. Souza, R. C. Michel, and B. G. Soares, "A methodology for studying the dependence of electrical resistivity with pressure in conducting composites," *Polym. Test*, vol. 24, no. 8, pp. 998–1004, 2005.
[20] J. R. Lu, X. F. Chen, and W. Lu, "The piezoresistive behaviors of polyethylene/foliated graphite nanocomposites," *Eur. Polym. J.*, vol. 42, pp. 1051–1021, 2006.
[21] S. Y. Qu and S. C. Wong, "Piezoresistive behavior of polymer reinforced by expanded graphite," *Compos. Sci. Technol.*, vol. 67, pp. 231–237, 2007.
[22] E. So, H. Zhang, and Y. S. Guan, "Sensing contact with analog resistive technology," in *Proc. IEEE Int. Conf. Syst., Man, Cybern.*, Tokyo, Japan, 1999, pp. 806–811.
[23] M. Shinmojo, R. Makino, A. Namiki, M. Ishikawa, T. Suzuki, and K. Mabuchi, "A sheet type tactile sensor using pressure conductive rubber with electrical-wires stitches method," in *Proc. IEEE Sensors*, , , 2002, pp. 1637–1642.
[24] M. Knite, V. Teteris, A. Kiploka, and J. Kaupuzs, "Polyisoprene-carbon black nanocomposites as tensile strain and pressure sensor materials," *Sens Actuators A, Phys.*, vol. 110, pp. 142–149, 2004.
[25] W. E. Mahmoud, A. M. Y. El-Lawindy, M. H. El-Eraki, and H. H. Hassan, "Butadiene acrylonitrile rubber loaded fast extrusion furnace black as a compressive strain and pressure sensors," *Sens Actuators A, Phys.*, vol. 136, no. 1, pp. 229–233, 2007.
[26] A. E. Job, F. A. Oliveira, N. Alves, J. A. Giacometti, and L. H. C. Mattoso, "Conductive composites of natural rubber and carbon black for pressure sensors," *Synth. Met*, vol. 135, pp. 99–100, 2003.
[27] A. C. Clark, S. P. Ho, and M. Laberge, "Conductive composite of UHMWPE and CB as a dynamic contact analysis sensor," *Tribol. Int.*, vol. 39, no. 11, pp. 1327–1335, 2006.
[28] L. Flandin, Y. Bréchet, and J. Y. Cavaillé, "Electrically conductive polymer nanocomposites as deformation sensors," *Compos. Sci. Technol.*, vol. 61, pp. 895–901, 2001.
[29] L. H. Wang, T. H. Ding, and P. Wang, "Effects of instantaneous compression pressure on electrical resistance of carbon black filled silicone rubber composite during compressive stress relaxation," *Compos. Sci. Technol.*, vol. 68, pp. 3448–3450, 2008.
[30] Y. J. Zhu, *Mechanical Modification of Elastomers—Filler Reinforcement and Blending*. Beijing, China: Science and Technology Press, 1992.
[31] X. S. Yi, *Function Principle of Filled Conductive Polymer Composites*. Beijing, China: National Defence Industry Press, 2004.

Luheng Wang received the Ph.D. degree from the Department of Precision Instruments and Mechanology, Tsinghua University, Beijing, China.

He is currently an Associate Professor with the College of Information Science and Engineering, Northeastern University, Shenyang, China. His current research interests include sensor fabrication, electronic skin development, failure detection and data recovery of multisensors based on artificial neural network, data fusion of multisensors based on expert system, and study on inner structure and properties of nanocomposite.

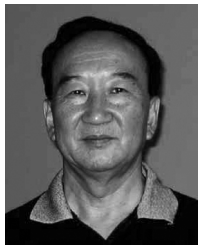

Tianhuai Ding received the B.Sc. degree in precision instruments from Tsinghua University, Beijing, China, in 1970.

From 1984 to 1986, he was an Associate Researcher at the University of Munich, Munich, Germany. He is currently a Professor with the Department of Precision Instruments and Mechanology, Tsinghua University, China. His current research interest is the study and development of the sensor.

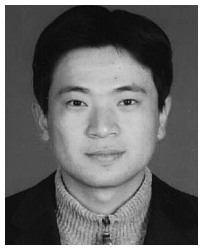

Peng Wang received the Ph.D. degree from the Department of Precision Instruments and Mechanology, Tsinghua University, Beijing, China.

He is currently with the Department of Precision Instruments and Mechanology, Tsinghua University, China. His current research interests is sensor development.